Original article

doi:10.5633/amm.2026.0109

FINITE ELEMENT ANALYSIS USED IN COMPARISON OF EXTRAMEDULLARY AND

INTRAMEDULLARY FIXATION OF PERTROCHANTERIC FRACTURES

Igor Merdzanoski<sup>1</sup>, Milan Mitkovic<sup>2,3</sup>, Ivan Mickoski<sup>4</sup>, Ile Mirceski<sup>4</sup>, Marko Spasov<sup>1,5</sup>

<sup>1</sup>University Clinic of Traumatology, Orthopedic Diseases, Anesthesia, Resuscitation, Intensive

Care and Emergency Center (TOARILUC), Clinical Center "Mother Teresa", Skopje, North

Macedonia

<sup>2</sup>Clinic for Orthopaedics and Traumatology "Academician Prof. Dr. Milorad Mitković", University

Clinical Center Nis, Nis, Serbia

<sup>3</sup>Faculty of Medicine, University of Nis, Nis, Serbia

<sup>4</sup>Faculty of Mechanical Engineering, University "Ss. Cyril and Methodius" in Skopje, Skopje,

North Macedonia

<sup>5</sup>Faculty of Medicine, University "Ss. Cyril and Methodius" in Skopje, Skopje, North Macedonia

Contact: **Igor Merdzanoski** 

105 Zivko Brajkovski St., 1230 Gostivar, North Macedonia

E-mail: igormerganoski@hotmail.com

Finite element analysis (FEA) has been the tool used for biomechanical stability analysis

in different types of pertrochanteric fractures fixation. Such biomechanical testing has

demonstrated its value in enhancing clinical treatment and in the development of osteosynthesis

implants. A biomechanical virtual testing of two designs with different geometrical structures of

osteosynthesis implants are being presented in this paper. The objective of this study was to

develop virtual models and analyze stress distribution and deformation in the femur using two

types of implants. Specifically, the study compares two fixation methods for intertrochanteric

femoral fractures: extramedullary fixation with an angled plate (DHS), and intramedullary

osteosynthesis using a trapezoidal nail with integrated interlocking via two screws (InterTAN). A

geometric model was developed to satisfy two key criteria: it provided sufficient detail for

1

comparative analysis, while also ensuring the precision required for a qualitative structural assessment. Additionally, a finite element model was constructed to support the numerical simulations. These simulations were performed to evaluate stress distribution and the stabilized positioning of the femur following osteosynthesis fixation with the selected implants. The results confirmed higher maximum stress and higher maximum deformation in analyzed pertrochanteric fracture fixation by DHS, comparing to InterTAN. In this way, other shapes of trochanteric fractures, for different body weights, could be analzed as well in order to properly assess the stability of the fixation method used.

**Keywords**: Finite element analysis; pertrochanteric fracture; stress distribution

Originalni rad

doi:10.5633/amm.2026.0109

PRIMENA METODE KONAČNIH ELEMANATA U ANALIZI EKSTRAMEDULARNE I INTRAMEDULARNE FIKSACIJE PERTROHANTERNIH PRELOMA

Igor Merdžanoski<sup>1</sup>, Milan Mitković<sup>2,3</sup>, Ivan Mickoski<sup>4</sup>, Ile Mirčeski<sup>4</sup>, Marko Spasov<sup>1,5</sup>

<sup>1</sup>Univerzitetska klinika za traumatologiju, ortopedske bolesti, anesteziju, reanimaciju, intenzivnu

terapiju i urgentni centar (TOARILUC), Klinički centar "Majka Tereza", Skoplje, Severna

Makedonija

<sup>2</sup>Klinika za ortopediju i traumatologiju "Akademik prof. dr Milorad Mitković", Univerzitetski

klinički centar Niš, Niš, Srbija

<sup>3</sup>Medicinski fakultet, Univerzitet u Nišu, Niš, Srbija

<sup>4</sup>Mašinski fakultet, Univerzitet "Sv. Ćirilo i Metodije" u Skoplju, Skoplje, Severna Makedonija

<sup>5</sup>Medicinski fakultet, Univerzitet "Sv. Ćirilo i Metodije" u Skoplju, Skoplje, Severna Makedonija

Kontakt: **Igor Merdžanoski** 

Živko Brajkovski 105, 1230 Gostivar, Severna Makedonija

E-mail: igormerganoski@hotmail.com

Analiza konačnih elemenata (Finite element analysis - FEA) se može koristiti u proceni

biomehaničke stabilnosti kod različitih vrsta fiksacije pertrohanternih preloma. Ovakvo

biomehaničko ispitivanje pokazuje svoj značaj u unapredjenju kliničkog lečenja, kao i u razvoju

samih osteosintetskih implantata. U ovom radu je predstavljeno biomehaničko virtuelno testiranje

dva implantata sa različitim geometrijskim karakteristikama. Cilj ove studije bio je razvoj virtuelnih

modela i analiza raspodele napona i deformacije u butnoj kosti korišćenjem dva tipa implantata.

U ovoj studiji se upoređuju dve metode fiksacije za trohanterne prelome femura: ekstramedularna

fiksacija ugaonom pločom sa kliznim zavrtnjem (DHS) i intramedularna fiksacija korišćenjem klina

sa trapezoidnim poprečnim presekom i sa dva kllizna zavrtnja koji su u medjusobnom kontaktu

(InterTAN). Geometrijski model je razvijen tako da zadovolji dva ključna kriterijuma: pružio je

3

dovoljno detalja za uporednu analizu, a istovremeno je osigurao preciznost potrebnu za kvalitativnu strukturnu procenu. Pored toga, konstruisan je i model konačnih elemenata kao podrška numeričkim simulacijama. Ove simulacije su izvršene da bi se procenila raspodela napona pri stabilizaciji preloma sa odabranim implantatima. Rezultati su potvrdili veći maksimalni napon i veću maksimalnu deformaciju kod analizirane fiksacije pertrohanternih preloma pomoću DHS-a, u poređenju sa InterTAN-om. Na ovaj način, mogli bi se analizirati i drugi oblici trohanternih preloma, za različite telesne težine, kako bi se pravilno procenila stabilnost korišćene metode fiksacije.

Ključne reči: analiza konačnih elemenata; pertrohanterni prelomi; stress distribution

## **INTRODUCTION**

Globally, around 1.5 million hip fractures occur each year, and this figure is projected to rise to 6.3 million by the year 2050 [1]. Pertrochanteric fractures, as a type of osteoporotic hip fractures, represent approximately half of hip fractures [2,3]. Internal fixation of such fractures is followed by a rate of complications, with one-year post-surgical mortality rate ranging from 14% to 36% [4]. Pertrochanteric fractures are the type of trochanteric fractures, extending from the greater trochanter to the lesser trochanter of the femur [5,6].

Finite elements analysis is a useful method to assess the stability of any fracture treated by a certain implant. Given the increased mechanical load that prevails in the hip joint, finite element analysus had been performed on different fixation methods used in femoral neck fractures treatment [7]. The authors developed a plate-termed the Slide Compression Anatomic Plate for the Femoral Neck (SCAP-FN) which integrates the mechanical advantages of both cannulated screws and a sliding hip screw. This design features three dynamic screws fixed at an angle and attached to a side plate. Finite element analyses (FEA) were conducted to evaluate the performance of the SCAP-FN in comparison with the dynamic hip screw combined with a derotational screw (DHS+DS) and with cannulated screws alone. Some authors had developed virtual model based on anatomical reduction data from a clinical patient case, using FEA [8]. The model was subjected to physiological loading conditions to analyze the resulting biomechanical responses in various regions. Jiantao Li et al. had performed a comparative biomechanical study of the Medial Sustainable Nail (MSN) and the Proximal Femoral Nail Antirotation (PFNA) for the treatment of AO/OTA 31-A2.3 fractures [9]. In addition to the simulation, biomechanical experiments were used to evaluate axial stiffness and performance under cyclic axial loading as well. Radek Bartoska et al. utilized a numerical model and finite element analysis to investigate various positioning scenarios of intramedullary nails (IMHN/PFH) in the proximal femur [10]. The study aimed to identify implant positions that are more prone to mechanical failure, thereby providing insights into optimal placement for improved fixation stability.

Li et al. had used FEA in the von Mises stress analysis, along with maximum and minimum principal stresses, were to assess bone ingrowth influence on stress distribution in the proximal femur post-fixation in 31A1 trochanteric fractures [11].

The aim of this study was to perform biomechanical virtual testing of two implants (DHS an InterTAN) with different geometrical structures in the treatment of AO/OTA A1 pertrochanteric

fracture, by developing virtual models and analyzing the stress distribution and deformation in the proximal femur.

### **MATERIALS AND METHODS**

For the purpose of virtual testing by FEA, the upper half of the femur, including an pertrochanteric fracture, was modeled. The femur model was defined to have an inner cancellous bone layer surrounded by a cortical bone shell with a thickness ranging from 4 to 7 mm. In the finite element model, both cancellous and cortical bone were assumed to be linear, elastic, and homogeneous materials. The elastic modulus (Young's modulus) of cancellous bone typically ranges from 1.5 to 3 GPa; in this model, it was set to 3 GPa with a Poisson's ratio of 0.3. For the cortical bone, the elastic modulus was defined as 20 GPa, also with a Poisson's ratio of 0.3. The cortical layer, which forms a dense outer shell, is the strongest part of the bone, composed of approximately 95% mineral salts.

All materials used in the finite element model were assumed to be linear, elastic, and homogeneous. Titanium alloy (Ti-6Al-4V) and stainless steel (SS316L) are biocompatible materials widely used in orthopedic implants due to their excellent corrosion resistance, non-toxic nature, and favorable mechanical properties. Additionally, titanium alloy is non-magnetic, making it particularly suitable for medical applications. Among titanium-based and stainless-steel materials, Ti-6Al-4V and SS316L are the most commonly used for implant applications. In this study, both Ti-6Al-4V alloy and stainless steel (SS316L) were employed.

A reverse engineering approach was employed to generate a 3D model of the femur bone from computed tomography (CT) data. CT scanning was performed using a Siemens spiral CT scanner with a slice thickness of 2 mm. A three-dimensional solid model of the femur bone was created using specialized medical image processing software. The resulting virtual stereolithographic (STL) model was refined using various masks and filters to accurately preserve the anatomical features of the bone. This STL model was then converted into a solid model using the CAD software package SolidWorks. The software package SolidWorks Simulation was used to perform the finite element analysis and virtual testing. The resulting 3D model and the corresponding finite element analysis (FEA) mesh are shown in Figure 1.

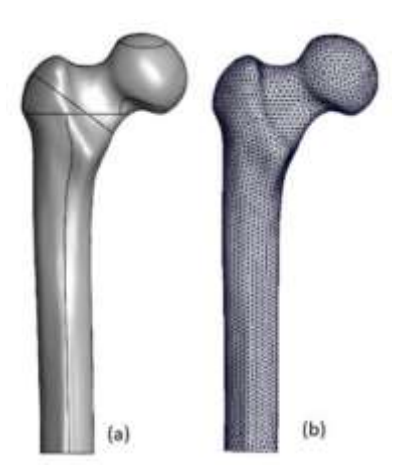


Figure 1. Femur bone model: 3D model (a) and 3D mesh model (b)

In this research, two different fixation methods for pertrochanteric femoral fractures were selected: extramedullary fixation by an angled plate with a single helical-threaded lag screw (DHS), and extramedullary fixation by an trapezoidal nail with integrated interlocking through two connected sliding screws (InterTAN). In the finite element analysis, the screws were defined in a simplified form.

The models contain multiple components in contact with one another. To accurately simulate these interactions, several contact pairs were defined: screw-bone, screw-implant body, implant body-screw, screw-implant body, screw-bone, and bone-bone. Table 1 presents the coefficient of friction values corresponding to various contact pairs.

Table 1. Coefficient of friction values for various contact pair types.

Contact pairs	Coefficient of friction - µ
metal-metal	0.15
bone-metal	0.30
bone-bone	0.50

The study was performed in two stages. In the first stage, a preliminary axial tightening force was applied to the compression screw. In the second stage, this preload was maintained, and an additional vertical load was applied to the system (Fig. 2). To perform the first stage of the analysis, it was necessary to determine the appropriate preload force for the compression screw. Using tabulated data for this thread type and strength class, the required axial tightening

force was determined to be 1710 N (according to ISO 965-2 standard), which ensures that the femoral screw can effectively compress the fractured bone fragments along the fracture plane.

To calculate the total force acting on the upper hemisphere of the femoral head, the dynamic biomechanical model of the leg system was created. The dynamic biomechanical model schematically is represented in Figure 2. The biomechanical model consists of pelvis, hip joint, femur bone, knee joint, shinbone and contact of foot with ground.

# Geomtric model analyzis of the hip load during the gait

Q – ground reaction force acting on the foot

 $Q_x$  – projection of the ground reaction force on the x – axis

 ${\it Q}_{\it y}$  – projection of the ground reaction force on the y – axis

 $m_h$  – body weight

 $m_f$  – femur weight

 $m_s$  – shinbone (lower leg) weight

 $l_b$  – body height

 $l_f$  – femur height

 $l_s$  – shinbone (tibia) height

lpha — the angle between the body and the vertical Y-axis, which varies during gait and changes over time lpha=lpha(t)

 $\beta$  – the angle between the femur and the vertical Y-axis, which varies over time  $\beta = \beta(t)$ 

 $\gamma$  – the angle between the shinbone (tibia) and the vertical Y-axis, which varies over time  $\gamma = \gamma(t)$ 

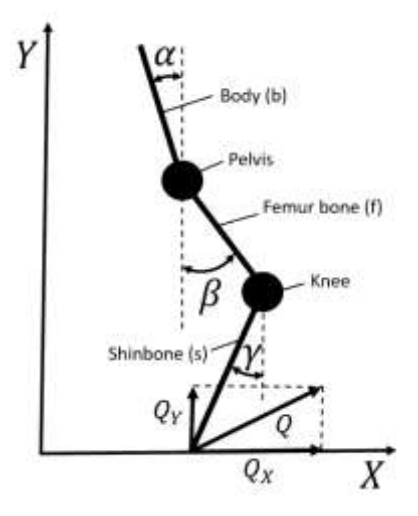


Figure 2. Dynamic biomechanical model of the pelvis-hip joint-femur-knee joint-shinbone system

The moment of inertia of the patient's body relative to the ground reference frame:

$$J_b = \frac{1}{2} (m_b + m_f + m_s) \left( \frac{l_b}{2} + l_f + l_s \right)^2$$

The moment of inertia of the patient's femur relative to the ground reference frame:

$$J_f = \frac{1}{12} (m_f + m_s) \left( \frac{l_f}{2} + l_s \right)^2$$

The moment of inertia of the patient's shinbone relative to the ground reference frame:

$$J_s = \frac{1}{12} m_s \left(\frac{l_s}{2}\right)^2$$

Variation of the foot's x and y coordinates in accordance with the dynamic model presented in Figure 2:

$$x = x_0 - l_f \sin\beta + l_s \sin\gamma \tag{1}$$

$$y = l_f cos\beta + l_s cos\gamma \tag{2}$$

The x and y coordinates of the foot change over time.

The ground reaction force acting on the foot can be calculated by equation:

$$Q = \sqrt{Q_x^2 + Q_y^2} \tag{3}$$

The values of  $\ddot{x_c}$  and  $\ddot{y_c}$  are calculated from the differential equations of motion of the center of mass of the system shown in figure 6:

$$\dot{x_c} = \frac{Q_x}{m_b + m_f + m_S} \tag{4}$$

$$\ddot{y_c} = \frac{Q_y - (m_b + m_f + m_s)g}{m_b + m_f + m_s} \tag{5}$$

The coordinates  $x_c$  and  $y_c$  of the center of mass of the considered system shown in Figure 2 depends on time and are calculated using the following equations:

$$x_c = \frac{x(m_b + m_f + m_s) - m_b r_b \sin\alpha + m_f r_f \sin\beta - m_s r_s \sin\gamma}{m_b + m_f + m_s}$$
(6)

$$y_c = \frac{y(m_b + m_f + m_s) - m_b r_b \cos\alpha + m_f r_f \cos\beta - m_s r_s \cos\gamma}{m_b + m_f + m_s}$$
(7)

The varialbes  $r_b$ ,  $r_f$  and  $r_s$  represents distances between hip joint and center of the body mass, femur, and shinbone; g represents acceleration due to gravity.

In the analysis of the dynamic system presented in Figure 2, particular attention is given to the force acting on the femur bone. These force vary in both magnitude and direction throughout the gait cycle and is time-dependent. To compute force acting on the femur, the Lagrangian equations of motion are employed. The forces on the femur and shinbone cannot be analyzed in isolation; they must be considered in conjunction with the forces acting on the body during walking. The force acting on the femur can be determined using the following equation:

$$F_f = J_f \ddot{\beta} - r_f (m_f + m_s) (g + \ddot{x} cos\beta + \ddot{y} sin\beta) + r_s m_s (\ddot{\gamma} cos(\beta - \gamma) - \dot{\gamma}^2 sin(\beta - \gamma))$$
 (8)

The force  $F_f$  exerted on the femur bone is transferred to the hip joint and exhibits time-dependent variations in both magnitude and direction over an 8-second duration.

The force acting on the shinbone can be determined using the following equation:

$$F_s = J_s \ddot{\gamma} - r_f m_s \left( g sin \gamma + (\ddot{x} cos \gamma + \ddot{y} sin \gamma) \right) + \left( \ddot{\beta} cos (\beta - \gamma) - \dot{\beta} sin (\beta - \gamma) \right)$$
 (9)

To fully characterize the dynamics of the system illustrated in Figure 2, we derive expressions for the kinetic energy  $(E_k)$  and potential energy  $(E_p)$  as follows:

$$E_{k} = \frac{1}{2} \left( m_{b} + m_{f} + m_{s} \right) (\dot{x}^{2} + \dot{y}^{2}) - r_{b} \dot{x} (\dot{x} \cos \alpha + y \sin \alpha) + \frac{1}{2} \left( J_{b} \alpha^{2} + J_{f} \beta^{2} + J_{s} \gamma^{2} \right) + \left( J_{f} + J_{s} \right) \dot{\beta} \dot{\gamma} \cos(\beta \gamma) + r_{s} \left( m_{f} + m_{s} \right) (\dot{x} \cos \beta + \dot{y} \sin \beta) + r_{s} m_{s} \dot{\gamma} (\dot{x} \cos \gamma + \dot{y} \sin \gamma)$$

$$\tag{10}$$

$$E_p = g(m_b + m_f + m_s)(y + r_b cos\alpha) - g(r_f(m_f + m_s)cos\beta - r_s m_s cos\gamma)$$
(11)

The dynamics and motion of the system illustrated in Figure 2 are described by Equations (1) through (11).

By solving differential equations (4) and (5) with initial conditions  $x_0 = 0$ ;  $y_0 = 0$  and assuming  $a(t) \rightarrow 0$  (where a is small, approximately in the range of 6 to  $8^{\circ}$ ), we derive the following equations:

$$\left(\frac{m_f r_f}{m_b + m_f + m_s} - l_f\right) \left(\ddot{\beta} \cos\beta - \dot{\beta} \sin\beta\right) + \left(l_s - \frac{m_s r_s}{m_b + m_f + m_s}\right) \left(\ddot{\gamma} \cos\gamma - \dot{\gamma} \sin\gamma\right) = \frac{Q_\chi}{m_b + m_f + m_s} \tag{12}$$

$$\left(l_f - \frac{m_f r_f}{m_b + m_f + m_s}\right) \left(-\ddot{\beta} \sin\beta - \dot{\beta} \cos\beta\right) + \left(l_s - \frac{m_s r_s}{m_b + m_f + m_s}\right) \left(-\ddot{\gamma} \cos\gamma - \dot{\gamma} \sin\gamma\right) = \frac{Q_y}{m_b + m_f + m_s} \tag{13}$$

For patients with 90 kg body weight and 180 cm height ( $m_f$ =12,971kg;  $m_s$ =3,831kg;  $l_f$ =0,495m;  $l_s$ =0,4059m;  $r_f$ =0,2178m;  $r_s$ =0,168m;  $J_f$ =0,5977 Nm²), the equations (12) and (13) will be represented in simplified form:

$$-0.36(\ddot{\beta}\cos\beta - \dot{\beta}\sin\beta) - 0.42(\ddot{\gamma}\cos\gamma - \dot{\gamma}\sin\gamma) = 1.27 \tag{14}$$

$$0.36(-\ddot{\beta}\sin\beta - \dot{\beta}\cos\beta) - 0.42(-\ddot{\gamma}\sin\gamma - \dot{\gamma}\cos\gamma) = 1.27$$
 (15)

Initial conditions:

$$\beta(0) = 0 \text{ and } \gamma(0) = 0 \tag{16}$$

$$\dot{\beta}(0) = 0 \text{ and } \dot{\gamma}(0) = 0$$
 (17)

By solving the system of equations (14) and (15) and using initial conditions given by equations (16) and (17), will be obtain values for the angles  $\beta$  and  $\gamma$ , representing the changes of the femur bone and shinbone during an 8-second walking period. The MATLAB/Simulink software package and the corresponding Simulink block diagram are used to solve equations (14) and (15), using the initial conditions defined in (16) and (17). The Simulink block diagram presented in Figure 3 is used to compute the angles  $\beta$  and  $\gamma$  for a patient weighing 90 kg and measuring 180 cm in height.

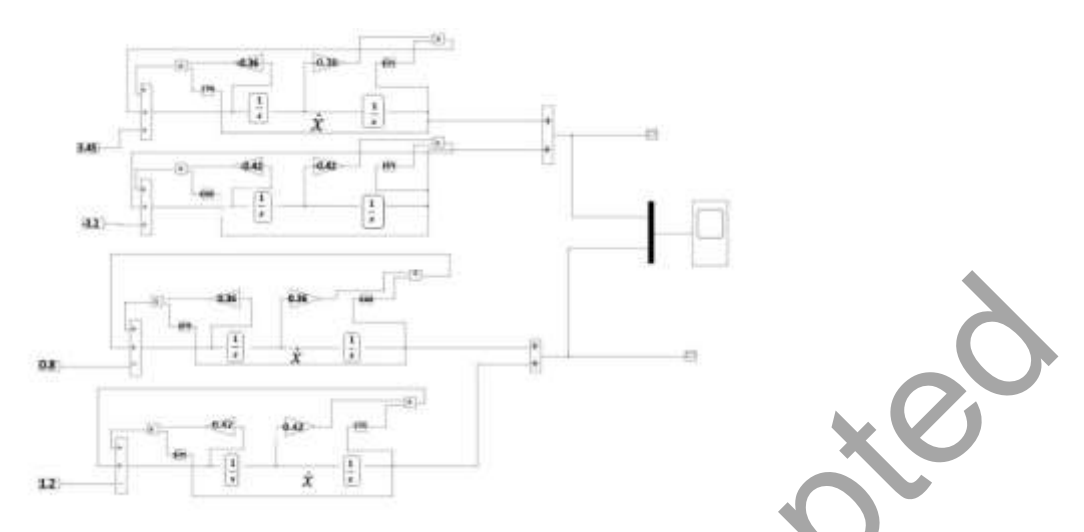


Figure 3. Simulink block diagram for computing the angles  $\beta$  and  $\gamma$ .

In Figure 4 are presented results for angles  $\beta$  and  $\gamma$ , for a patient weighing 90 kg and measuring 180 cm in height. The following results were obtained:  $\beta$ =40° a 3a  $\gamma$ =0°÷5° u  $\gamma$ =5°÷(-60°).

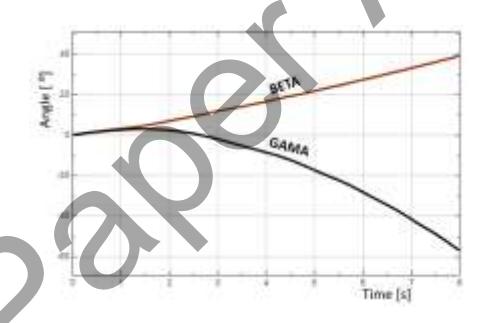


Figure 4. Diagram of variation of angles  $\beta$  and  $\gamma$ 

The MATLAB Simulink block diagram is used to solve equations (8). The Simulink block diagram presented in Figure 5 is used to compute the force acting on the femur  $F_f$ , for a patient weighing 90 kg and measuring 180 cm in height.

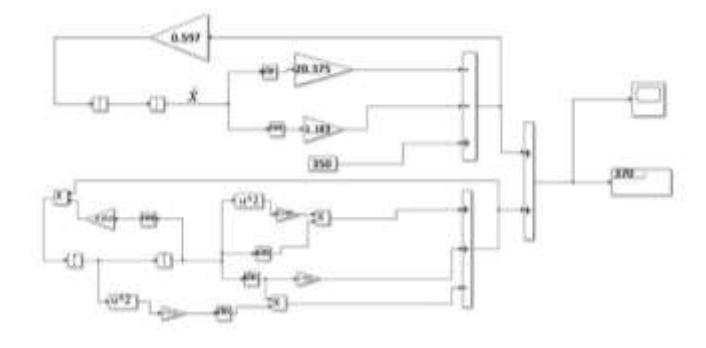


Figure 5. Simulink block diagram for computing of the force acting on the femur  $F_f$ .

# **RESULTS**

Results for the force acting on the femur  $F_f$ , for a patient weighing 90 kg and measuring 180 cm in height are presented in Figure 6.

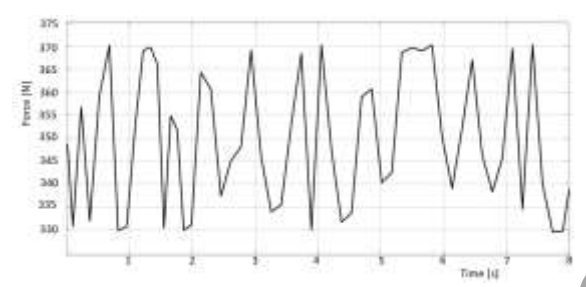


Figure 6. Diagram which shows the variation of the force acting on the femur  $F_f$ .

The maximum value of force acting on the femur was conducted to be 370 N. Accounting for additional forces from surrounding ligaments and muscles, the total force on the femoral head was defined as F = 400 N. During load application, the cylindrical end of the femur was rigidly fixed, and a uniformly distributed load was applied to the spherical surface of the femoral head (Fig. 7).

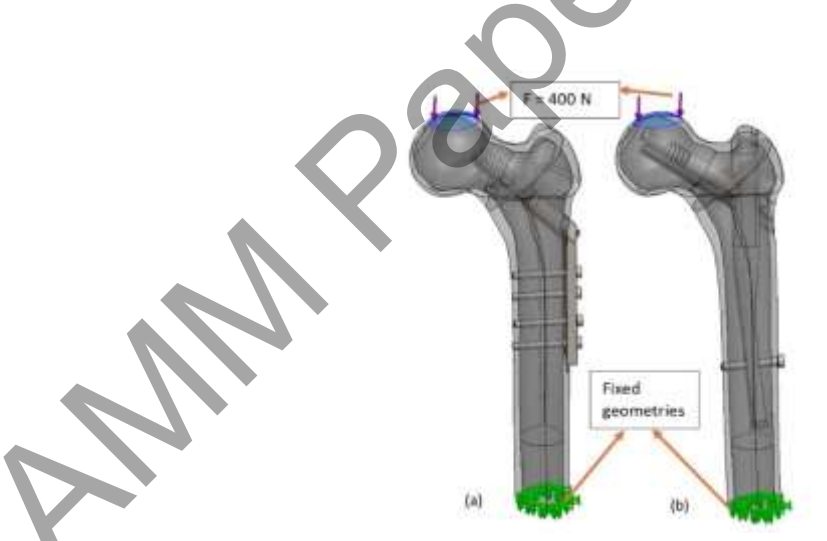


Figure 7. Initial and boundary conditions: (a) extramedullary fixation (b) intramedullary fixation.

There are presented Von Mises stress distribution in the cancellous bone, cortical bone of the femur, and the osteosynthesis implants (Figure 8), three-dimensional FEA of stress and deformation in cortical and cancellous bone (Figure 9), and stress distribution in both extramedullary (Figure 10) and intramedullary fixation (Figure 11). Moreover, maximu stress and deformation results in assemblies of the fixation (Table 2), cortical and cancellous bone (Table 3), and safety factors (Table 4) are being reported too.

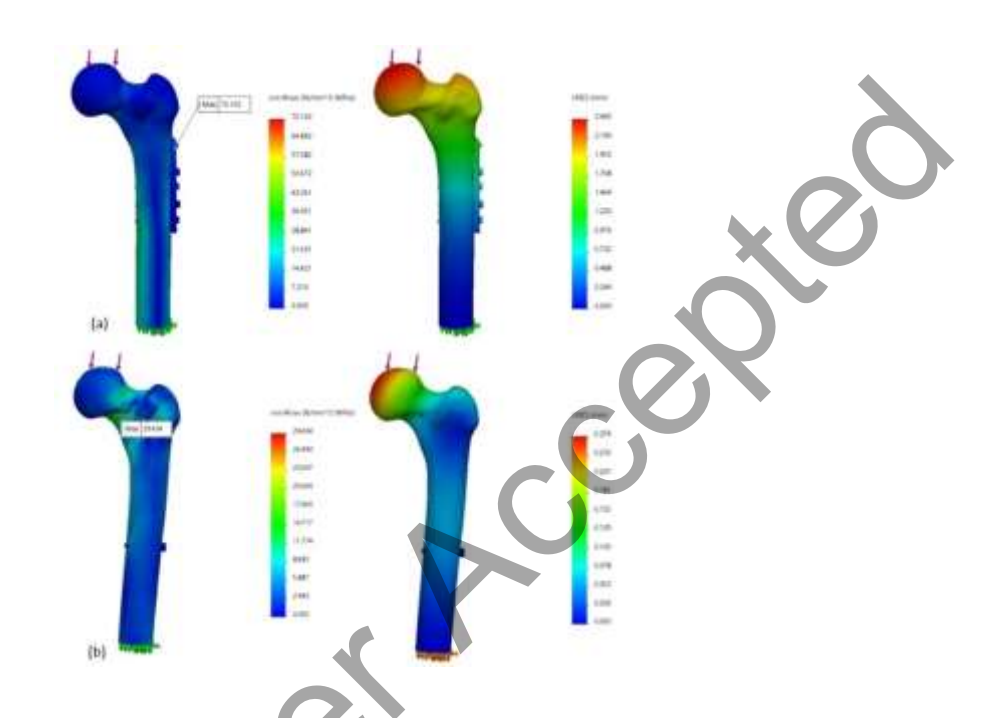


Figure 8. Three-dimensional FEA showing stress and deformation fields: (a) femoral assembly with DHS; (b) femoral assembly with InterTAN; stress units – Mega Pascals (MPa); displacement units – milimeters (mm).

Table 2. Results for the maximum stress and deformation values in assemblies both with extramedullary and intramedullary fixation.

	extramedullary fixation	Intramedullary fixation
	(DHS)	(InterTAN)
Maximum stress (MPa)	72.1	29.43
Maximum deformation (mm)	2.4	0.259

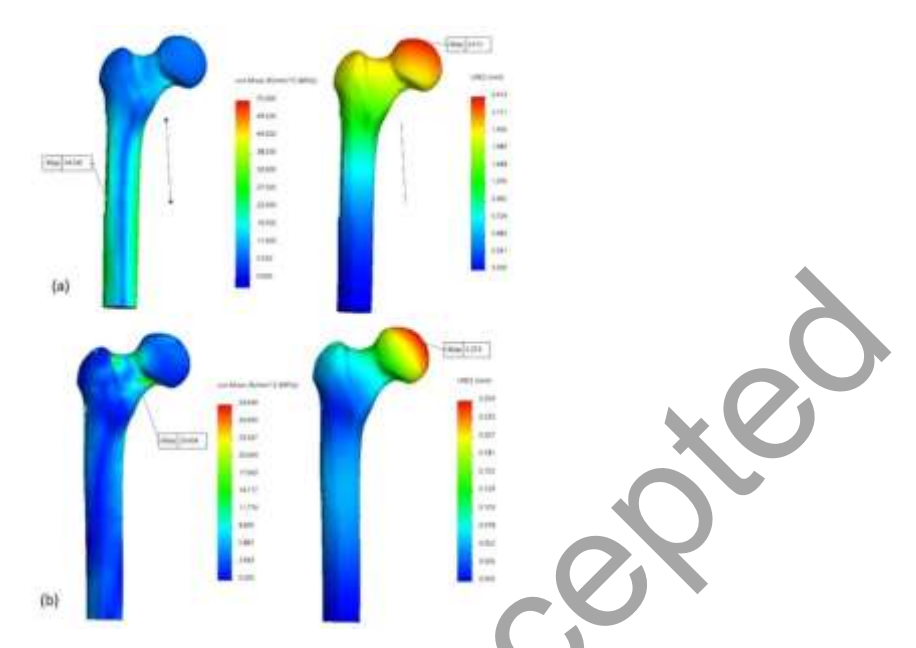


Figure 9. Three-dimensional FEA illustrating stress and deformation fields in cortical and cancellous bone: (a) with DHS; (b) with InterTAN.

Table 3. Results for the maximum stress and deformation values in both cortical and cancellous bone for extramedullary and intramedullary fixation implants.

	extramedullary fixation	Intramedullary fixation
	(DHS)	(InterTAN)
Maximum stress (MPa)	54.54	29.43
Maximum deformation (mm)	2.4	0.259

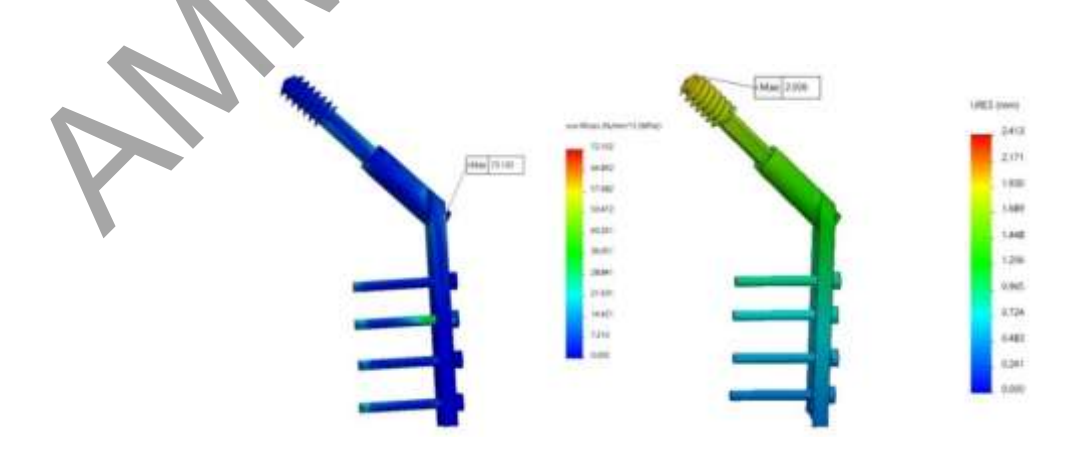


Figure 10. Three-dimensional FEA showing stress distribution in extramedullary fixation by DHS.

Table 4. Results for maximum stress, maximum deformation, and safety factors for both extramedullary and intramedullary fixation

	extramedullary fixation	Intramedullary fixation
	(DHS)	(InterTAN)
Maximum stress (MPa)	72.1	29.43
Maximum deformation	2	0.124
(mm)		
Safety factor	2.38	159

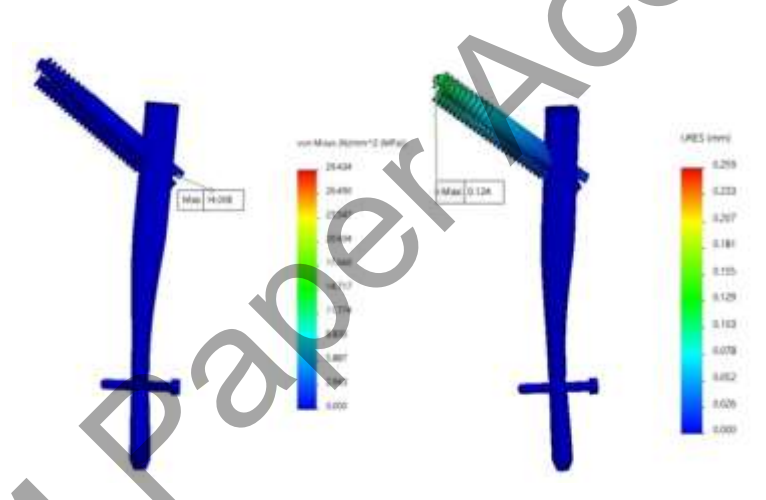


Figure 11. Three-dimensional FEA shows stress distribution in intramedullary fixation by InterTAN.

# **DISCUSSION**

The results presented below are based on the material properties of bone unaffected by osteoporosis. Figure 8 illustrates the stress and deformation fields in presented assembly for cases involving extramedullary and intramedullary fixation separately. The assembly with InterTAN fixation (Fig. 8b) showed better static behavior in relation to DHS fixation (Fig. 8a), according to maximum stress and maximum deformation values (Table 2).

When using extramedullary fixation with an angled plate (DHS), minor surface preparation and cutting of the cortical bone are required to ensure proper fitting of the implant plate. This adjustment leads to localized weakening of the bone in the area beneath the plate. The maximum stress occurs in the region where the cortical bone has been cut (Fig. 9). In contrast, the use of an intramedullary fixation by InterTAN requires significantly less cutting of the cortical bone. Reduced deformation (Table 3) is directly related to the minimal bone damage and limited cortical cutting associated with the internal osteosynthesis implant.

The yield strength of cortical bone was found to be 130 MPa [12]. Analyzing results in Table 3, there could be concluded that cortical bone is exposed for more damage, because the maximum stress and deformation values increase there. In both cases, the maximum stress and deformation values for both cortical and cancellous bone, when using extramedullary and intramedullary fixation implants, remain below the yield strength of cortical bone.

The use of a titanium alloy implant, compared to a stainless-steel implant, offers superior safety, with an exceptionally high safety factor.

The safety factor for the extramedullary fixation by an angled plate (2.38) confirms ensuring adequate patient safety using DHS. Considering the results of stress and deformation fields, intramedullary fixation also enhanced patient safety when using InterTAN.

Mahaisavariya et al. reported about comparison between intramedullary and extramedullary fixation of basocervical femoral fractures using FEA analysis. Basocervical femoral fractures are similar to pertrochanteric fractures. They also presented about generally higher implant body loads in DHS in relation to intramedullary nailing. But they found stress concentration around the contact between lag screw and the body of the intramedullary nail. It was notable in intersection planes of the nail model, not on the surface of the model. This could be considered the factor for the difference relating to our study [13].

Location and intensity of highest loads of the proximal femur found in our study are in accordance with Chen et al. who had used FEA in biomechanical investigation of a new cephalomedullary nail for trochanteric fractures [14].

There was no a longer gap between fracture fragments in out study. Bai et al. had performed FEA analyzis on a pertrochanteric fracture fixed by three different intramedullary nails, but there was a divergent gap between fracture fragments, that widened medially for several mm [15]. Such a gap could be considered to contribute for more clinically relevant results, because the fracture gap is never being with the full contact between the bone fragments in real. Bai et

al. also reported about the lowest stress in InterTAN. But, considering the study of Liao et al. who had compared two types pf intramedullary nails (PFNA and InterTAN), there was suggested still to conduct individualized assessments based on the patient's overall health status, surgical tolerance, and post-operative recovery needs, when choosing the implant for the fixation of a trochanteric fracture [16].

# **CONCLUSIONS**

Three-dimensional finite element analysis (FEA) provides virtual testing of different types of pertrochanteric fractures fixation. The created finite element models allow for the investigation of how the geometric dimensions and material properties of the components in both extramedullary and intramedullary fixation affect the overall stiffness of the system, while evaluating the influence of each component on the stability of bone fragments during the fracture healing. By comparing the calculated stresses with the material's yield strength, conclusions can be drawn regarding the structural integrity, and the safety factors can be determined. The satisfied results for stress and deformation are directly related to the minimal cortical bone damage. Virtual testing of fracture fixations gives a significant aid in new designs development, and determining potential locus minoris resistentiae. Implant body undergoes higher loads in DHS in relation to InterTAN, during the treatment od pertrochanteric fractures.

#### **REFERENCES**

- 1. Abrahamsen B, van Staa T, Ariely R, Olson M, Cooper C. Excess mortality following hip fracture: a systematic epidemiological review. Osteoporos Int. 2009; 20(10):1633–1650. DOI: 10.1007/s00198-009-0920-3
- 2. Imwinkelried T. Mechanical properties of open-pore titanium foam. J Biomed Mater Res Part A. 2007; 81:964–970.

DOI: 10.1002/jbm.a.31118

3. Wu HF, Chang CH, Wang GJ, Lai KA, Chen CH. Biomechanical investigation of dynamic hip screw and wire fixation on an unstable intertrochanteric fracture. Biomed Eng Online. 2019; 18:1–12.

DOI: 10.1186/s12938-019-0663-0

4. Lee C, Kelley B, Gurbani A, Stavrakis AI. Strategies for pertrochanteric fracture reduction and intramedullary nail placement: Technical tips and tricks. J Am Acad Orthop Surg. 2022; 30(18):867-878.

DOI: 10.5435/JAAOS-D-21-01007. PMID: 36166383.

5. Li J, Zhao Z, Yin P, Zhang L, Tang P. Comparison of three different internal fixation implants in treatment of femoral neck fracture-a finite element analysis. J Orthop Surg Res. 2019; 14(1):76.

DOI: 10.1186/s13018-019-1097-x.

6. Kim CJ, Lee JS, Goh TS, Shin WC, Lee C. Finite element analysis of fixation stability according to reduction position for internal fixation of intertrochanteric fractures. Sci Rep. 2024; 14(1):19214.

DOI: 10.1038/s41598-024-69783-9. PMID: 39160241; PMCID: PMC11333714.

7. Li J, Han L, Zhang H, Zhao Z, Su X, Zhou J, Li C, Yin P, Hao M, Wang K, Xu G, Zhang L, Zhang L, Tang P. Medial sustainable nail versus proximal femoral nail antirotation in treating AO/OTA 31-A2.3 fractures: Finite element analysis and biomechanical evaluation. Injury. 2019; 50(3):648-656.

DOI: 10.1016/j.injury.2019.02.008.

- 8. Bartoska R, Baca V, Horak Z, Hrubina M, Skala-Rosenbaum J, Marvan J, Kachlik D, Dzupa V. The importance of intramedullary hip nail positioning during implantation for stable pertrochanteric fractures: biomechanical analysis. Surg Radiol Anat. 2016; 38(5):577-585. DOI: 10.1007/s00276-015-1595-4.
- Li M, Zhao K, Ding K, Cui YW, Cheng XD, Yang WJ, Hou ZY, Zhang YZ, Chen W, Hu P, Zhu YB. Titanium Alloy Gamma Nail versus Biodegradable Magnesium Alloy Bionic Gamma Nail for Treating Intertrochanteric Fractures: A Finite Element Analysis. Orthop Surg. 2021; 13(5):1513-1520.

DOI: 10.1111/os.12973.

10. Morgan EF, Unnikrisnan GU, Hussein AI. Bone mechanical properties in healthy and diseased states. Annu Rev Biomed Eng. 2018; 4(20):119-143.

DOI: 10.1146/annurev-bioeng-062117-121139.

11. Mahaisavariya C, Jitprapaikulsarn S, Mahaisavariya B, Chantarapanich N. Torsional stability of fixation methods in basicervical femoral neck fractures: a biomechanical study. J Orthop Surg Res. 2024; 19(1):371.

- DOI: 10.1186/s13018-024-04842-5
- 12. Chen P, Fan Z, Xu N, Wang H. A biomechanical investigation of a novel intramedullary nail used to salvage failed internal fixations in intertrochanteric fractures. J Orthop Surg Res. 2023; 18(1):632.
  - DOI: 10.1186/s13018-023-04112-w. PMID: 37641046. PMCID: PMC10463605.
- 13. Bai H, Liu L, Duan N, Xue H, Sun L, Li M, Li Z, Zhang K, Wang Q, Huang Q. Biomechanical evaluation of three implants for treating unstable femoral intertrochanteric fractures: finite element analysis in axial, bending and torsion loads. Front Bioeng Biotechnol. 2023 Nov 7;11:1279067.
  - DOI: 10.3389/fbioe.2023.1279067. PMID: 38026862; PMCID: PMC10661970.
- 14. Liao CS, He FZ, Li XY, Han PF. Proximal femoral nail antirotation versus InterTan nail for the treatment of intertrochanteric fractures: A systematic review and meta-analysis. PLoS One. 2024 Jul 9;19(7):e0304654.
  - DOI: 10.1371/journal.pone.0304654. PMID: 38980889; PMCID: PMC11233004.
- 15. Srećković V, Stanković B, Krajinović A, Kovačević M, Jeremić D, Vukićević A, Živanović P. Surgical treatment of trochanteric fractures by Gamma3 nail. Acta Medica Medianae. 2010; 493:27-31.
  - UDC: 616.718.4-001.5-089
- 16. Grubor P; Asotić M, Grubor M. Method of choice in the treatment of femoral neck fractures in subjects aged over 65. Acta Medica Medianae. 2010; 49(3):5-10. UDC: 616.718.4-001.5-089.28:616-053.9